PLOS CLIMATE

RESEARCH ARTICLE

Carbon and carbon-13 in the preindustrial and glacial ocean

Andreas Schmittner*, Nathaniel J. Fillman

College of Earth, Ocean and Atmospheric Sciences, Oregon State University, Corvallis, Oregon, United States of America

* andreas.schmittner@oregonstate.edu

OPEN ACCESS

Citation: Schmittner A, Fillman NJ (2024) Carbon and carbon-13 in the preindustrial and glacial ocean. PLOS Clim 3(7): e0000434. https://doi.org/10.1371/journal.pclm.0000434

Editor: Matthieu Carré, Centre National de la Recherche Scientifique, FRANCE

Received: March 15, 2024

Accepted: June 4, 2024

Published: July 8, 2024

Data Availability Statement: Model code is available at https://doi.org/10.5281/zenodo.11224826 and at https://github.com/OSU-CEOAS-Schmittner/UVic2.9/releases/tag/v2.9.10. Input data files to run the PI simulation are available at https://doi.org/10.5281/zenodo.11226356. Input data files to run the LGM simulation are available at https://doi.org/10.5281/zenodo.11237025. Preindustrial D13C_DIC estimates (Kwon et al., 2022) were downloaded from https://climatedata.ibs.re.kr/data/papers/kwon-et-al-2022-commsenv. The uncertainties presented in Fig 2 (0.13 ‰) are the globally spatially averaged errors. PI and LGM D13C_DIC estimates from Gebbie et al. (2015)

Abstract

Despite their importance for Earth's climate and paleoceanography, the cycles of carbon (C) and its isotope ^{13}C in the ocean are not well understood. Models typically do not decompose C and ^{13}C storage caused by different physical, biological, and chemical processes, which makes interpreting results difficult. Consequently, basic observed features, such as the decreased carbon isotopic signature ($\delta^{13}C_{DIC}$) of the glacial ocean remain unexplained. Here, we review recent progress in decomposing Dissolved Inorganic Carbon (DIC) into preformed and regenerated components, extend a precise and complete decomposition to $\delta^{13}C_{DIC}$, and apply it to data-constrained model simulations of the Preindustrial (PI) and Last Glacial Maximum (LGM) oceans. Regenerated components, from respired soft-tissue organic matter and dissolved biogenic calcium carbonate, are reduced in the LGM, indicating a decrease in the active part of the biological pump. Preformed components increase carbon storage and decrease $\delta^{13}C_{DIC}$ by 0.55 ‰ in the LGM. We separate preformed into saturation and disequilibrium components, each of which have biological and physical contributions. Whereas the physical disequilibrium in the PI is negative for both DIC and $\delta^{13}C_{DIC}$, and changes little between climate states, the biological disequilibrium is positive for DIC but negative for $\delta^{13}C_{DIC}$, a pattern that is magnified in the LGM. The biological disequilibrium is the dominant driver of the increase in glacial ocean C and the decrease in $\delta^{13}C_{DIC}$, indicating a reduced sink of biological carbon. Overall, in the LGM, biological processes increase the ocean's DIC inventory by 355 Pg more than in the PI, reduce its mean $\delta^{13}C_{DIC}$ by an additional 0.52 ‰, and contribute 60 ppm to the lowering of atmospheric CO_2. Spatial distributions of the $\delta^{13}C_{DIC}$ components are presented. Commonly used approximations based on apparent oxygen utilization and phosphate are evaluated and shown to have large errors.

1. Introduction

The ocean's carbon cycle impacts atmospheric carbon dioxide (CO_2) and hence Earth's energy budget and climate [1]. Lower atmospheric CO_2 during glacial periods, for example, has been attributed to increased carbon storage in the ocean, although the mechanisms for the changes

were obtained from https://www2.whoi.edu/staff/ggebbie/.

Funding: This work was funded by the National Science Foundation of the United States of America grant number 1924215.

Competing interests: The authors have declared that no competing interests exist.

in ocean carbon remain controversial [2,3]. The isotopic ratio R = $^{13}C/^{12}C$, commonly expressed as$\delta^{13}C$ = (R/Rstd—1), that is the deviation from a standard ratio R_{std} (Equation A in S1 Text), is widely used in paleoceanography to trace past changes in carbon cycle and ocean circulation [4].

Understanding ocean C and ^{13}C cycling is complicated because they are influenced by different physical, chemical, and biological processes. As a gas, CO_2 dissolves is sea water and exchanges with the atmosphere. Solubility depends strongly on temperature [5], whereas the rate of air-sea flux is a function of wind speed [6]. Once in the ocean, CO_2 reacts with sea water and forms bicarbonate (HCO_3) and carbonate (CO_3) ions. At present-day pH levels, roughly 90% of the carbon is in bicarbonate form, about 10% is in CO_3 and only about 1% is CO_2 [7]; thus, the ocean is highly buffered with respect to CO_2. DIC = CO_2 + HCO_3 + CO_3 makes up the vast majority of ocean carbon (~37 Eg; 1 Eg = 10^{18} g = 10^3 Pg), whereas Dissolved Organic Carbon (DOC) amounts to ~0.7 Eg [8] and Particulate Organic Carbon (POC) is negligible in terms of global inventories. During air-sea gas exchange $\delta^{13}C$ fractionates such that the heavy isotope preferentially dissolves [7]. Isotopes are also fractionated between the different carbonate species, a process that is strongly temperature dependent [9]. As a result, at equilibrium, tropical DIC is enriched in ^{13}C with respect to atmospheric CO_2 by ~7.5 ‰ and polar DIC by ~10.5 ‰ [10], indicating that temperature changes can have an important impact on $\delta^{13}C_{DIC}$. Photosynthesis by phytoplankton removes carbon, preferentially ^{12}C, from surface waters creating POC and leaving surface waters depleted in DIC and enriched in $\delta^{13}C_{DIC}$ (~ +2 ‰). Calcifying organisms remove additional carbon from the surface together with alkalinity, but calcium carbonate production does not fractionate the isotopes. Eventually, sinking POC and calcium carbonate are returned to DIC in the subsurface ocean by respiration and dissolution, where it can be sequestered for centuries or longer. These processes are called the soft-tissue and carbonate pumps, terms coined in analogy to a cellular ion pump, which actively transports ions up gradient from lower to higher concentrations [11]. Together they are referred to as the biological carbon pump.

The biological pump continuously removes carbon from the surface to the deep ocean, thus contributing to lower atmospheric CO_2, and increasing DIC concentrations and decreasing $\delta^{13}C_{DIC}$ with depth. However, surface processes and transport of surface properties into the deep ocean also contribute to vertical variations in C and $\delta^{13}C_{DIC}$. Temperature-dependent solubility of C and fractionation of ^{13}C tends to increase the C content and $\delta^{13}C_{DIC}$ of polar waters, which fill the deep ocean and dominate the global inventory/average; this is the solubility pump [11]. Slow exchange with the atmosphere creates substantial disequilibria for both C and ^{13}C, which propagate into the interior [12–14]. On a global basis, the equilibration time with the atmosphere is about 1 year for C and 10 years for $\delta^{13}C_{DIC}$ [5,10], but it can be larger, e.g. in sea ice covered regions.

In principle, these processes are well known and represented in global ocean models. However, most ocean models only carry total DIC as a prognostic tracer, and thus cannot separately quantify how different processes contribute to a given change in DIC, which impedes interpreting and understanding DIC changes. Efforts to separate the different processes affecting DIC and $\delta^{13}C$ have a long history [10,11,15,16]. In models, biology can be switched off to simulate carbon in an abiotic ocean [11,13,14], however it is not often done to interpret results from a full model. Relationships between biological carbon and other substances involved in biological cycling such as phosphorous and oxygen have been used to estimate the contributions of biology. The storage of carbon from remineralization of organic matter $C_{soft} \cong C_{soft,AOU} = r_{C:O} \cdot AOU$, also known as the soft-tissue biological pump, has been suggested to be related to Apparent Oxygen Utilization (AOU = $O_{2,sat}$—O_2), which is the deviation of oxygen from its temperature-dependent saturation concentration $O_{2,sat}$ [17], using a constant carbon-

to-oxygen ratio $r_{C:O}$ [18–21]. Similarly, $C_{soft} \cong C_{soft,PO4} = r_{C:P} \cdot (PO_4 — PO_{4,0})$, the deviation of phosphate from a reference value such as the globally-averaged surface-mixed-layer concentration $PO_{4,0}$ has been used [11,16], assuming a constant carbon-to-phosphorous ratio ($r_{C:P}$). A popular approximation in paleoceanography attempts to isolate the effect of air-sea exchange, $\delta^{13}C_{as} = \delta^{13}C - (2.7–1.1 \times PO_4)$, by using phosphate to remove the effect of biology on $\delta^{13}C$ [10,15,22,23]. A recent variant is to use AOU to approximate $\delta^{13}C_{soft} \cong \delta^{13}C_{soft,AOU} = AOU \cdot (-1.1)/170$ [24]. However, all these approximations are problematic. Oxygen, notwithstanding its much shorter equilibration time with the atmosphere (~1 month) than carbon (~1 year), is substantially undersaturated in regions of deep water formation and the degree of undersaturation is time dependent, which can lead to large errors in the AOU approximation [25–27]. Similarly, preformed PO_4 shows substantial variations for different deep-water masses [28] and almost certainly has varied in time, which affects $\delta^{13}C_{as}$, as shown herein. Moreover, the ratio of carbon to phosphorous $r_{C:P}$ in organic matter is spatiotemporally variable [29,30].

Recently, models have started to include additional diagnostic tracers that can be used to decompose ocean carbon storage thereby avoiding the large errors associated with the above approximations [12,31,32]. These studies have emphasized the role of disequilibrium carbon storage C_{dis}, but they were incomplete, which hampered the interpretation of C_{dis}. Complete decompositions, separating C_{dis} into biological and physical contributions (Fig 1) has facilitated that interpretation and led to additional mechanistic insights into the modern and glacial ocean [1,2,33]. Here we extend a complete and accurate decomposition of DIC to $\delta^{13}C_{DIC}$.

$\delta^{13}C_{DIC}$ in past oceans can be reconstructed by measuring $\delta^{13}C_{cib}$ in shells of the fossil foraminifera genus *Cibicides* extracted from sediment cores [34]. Since $\delta^{13}C_{cib}$ is one of the most measured paleoceanographic tracers, a better understanding of $\delta^{13}C_{DIC}$ would benefit paleoceanography and Earth science in general. One of the best studied periods in paleoclimate is the Last Glacial Maximum (LGM, ~20,000 years ago), because climatic changes were large (good signal-to-noise ratio), and samples can be well dated with radiocarbon. Shackleton [35] first noted a decrease in ocean $\delta^{13}C_{DIC}$ during glacial periods, which he attributed to the transfer of isotopically light terrestrial organic carbon to the ocean. The general decrease in whole

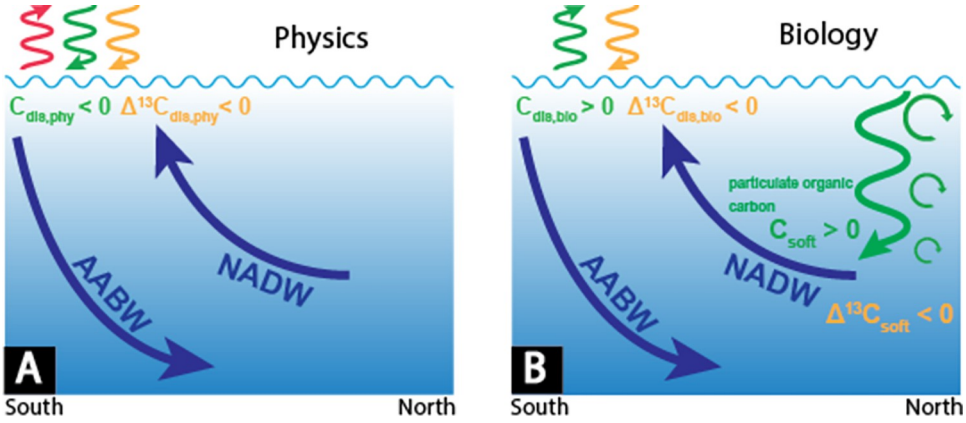

Fig 1. Disequilibrium schematic in Southern Ocean. In an ocean without biology (A) upwelling of North Atlantic Deep Water (NADW) occurs in the Antarctic divergence. Subsequent flow to the south leads to heat loss to the atmosphere (red wiggly line). This increases its solubility, which causes uptake of carbon (green wiggly line), and a surface flux that tends to increase $\delta^{13}C$ (orange wiggly line). However, due to incomplete air-sea gas exchange before waters sink to depths as Antarctic Bottom Water (AABW) negative disequilibria remain for both carbon and $\delta^{13}C$. Soft-tissue biology (B), conversely, causes upwelling of respired carbon that is depleted in $\delta^{13}C$, which leads to outgassing of carbon, but a surface flux that tends to increase $\delta^{13}C$. This results in a positive disequilibrium for carbon, but a negative disequilibrium for $\delta^{13}C$.

https://doi.org/10.1371/journal.pclm.0000434.g001

ocean $\delta^{13}C_{DIC}$ has subsequently been confirmed. The most recent study used hundreds of sediment cores combined with an inverse model to estimate a decrease in global mean ocean $\delta^{13}C_{DIC}$ of 0.32±0.20 ‰ in the LGM relative to the PI [36; G15]. An unequivocal interpretation of those observations, however, remains lacking. While a transfer of land carbon to the ocean is still a viable possibility [36,37], another possibility is an increase in the biological pump [3,38], which would decrease deep ocean and hence whole ocean $\delta^{13}C_{DIC} \cong \Delta^{13}C_{pre} + \Delta^{13}C_{soft}$. However, Sigman & Hain's [3] argument is based on an estimate by Vollmer et al. [24] of global ocean preformed $\Delta^{13}C_{pre}$ changes being close to zero, which used the AOU approximation. Moreover, in Khatiwala et al.'s [2; K19] data-constrained model, the biological pump (C_{soft}) was weaker during the LGM, whereas $C_{dis,bio}$ was greatly enhanced.

Here we build upon the modeling efforts mentioned above, specifically the work of K19. Those authors had implemented additional diagnostic tracers in an offline model, which was used to simulate LGM and PI equilibrium states. We have implemented a slightly modified method in an online model, which can be used for transient simulations, and we have extended the decomposition to $\delta^{13}C_{DIC}$. The latter has not been attempted before in the literature that we are aware of. We apply the method to data-constrained simulations of the PI and LGM oceans.

2. Model description

The Oregon State University version of the University of Victoria (OSU-UVic) climate model [39] includes a simple energy-moisture-balance atmospheric component, a land surface and dynamic vegetation model, a three-dimensional coarse-resolution ocean general circulation model component and the Model of Ocean Biogeochemistry and Isotopes (MOBI). MOBI features three phytoplankton functional types (diatoms, diazotrophs and other phytoplankton), nitrogen, phosphorous, silicate, and iron as growth-limiting nutrients, carbon, oxygen, zooplankton, detritus (POC), variable P:C ratios in phytoplankton, DOC, nitrogen (^{15}N) and carbon (^{13}C, ^{14}C) isotopes. Implementation of $\delta^{13}C$ is described in detail in Schmittner et al. [20]. The version used here does not include interactive sediments. OSU-UVic/MOBI has been validated against modern observations and against paleoceanographic data from the LGM [2,40–43]. Noticeable differences with previous versions are some details of the ocean ecosystem model such as the use of variable P:C ratios of phytoplankton, variable half-saturation constants for nutrient uptake, and different parameters [44]. Tracer distributions in the PI state are similar to previously published versions and agree well with observations, including DIC and $\delta^{13}C_{DIC}$ (Figs A-C and Section D in S1 Text). The LGM state used here is also very similar to K19 and agrees well with reconstructions of surface temperatures, whole ocean temperatures, $\delta^{13}C_{DIC}$, $\Delta^{14}C$ and $\delta^{15}N$, and features a shallower and weaker Atlantic Meridional Overturning Circulation (AMOC; Figs D-E and Section E in S1 Text) and enhanced iron fertilization in the Southern Ocean [41].

In addition to the prognostic equations for DIC and $DI^{13}C$ we have implemented equations for C_{pre}, C_{sat}, C_{soft}, C_{CaCO3}, $^{13}C_{pre}$, $^{13}C_{sat}$, $^{13}C_{soft}$, and $^{13}C_{CaCO3}$ (see Section A in S1 Text for notation). C_{pre} and $^{13}C_{pre}$ are set to DIC and $DI^{13}C$, respectively, in the surface layer and are transported into the subsurface. In contrast to DIC and $DI^{13}C$, however, for C_{pre} and $^{13}C_{pre}$ there are no interior sources and sinks from biology. C_{sat} and $^{13}C_{sat}$ are calculated as the DIC concentration in equilibrium with the atmosphere, implying no surface fluxes, with zero interior sources and sinks. The disequilibrium $C_{dis} = C_{pre} - C_{sat}$ is diagnosed. C_{soft} (C_{CaCO3}) and $^{13}C_{soft}$ ($^{13}C_{CaCO3}$) are set to zero at the surface and in the subsurface they are subject to the same sources and sinks as DIC related to the production and regeneration of organic matter

($CaCO_3$). To separate biological and physical effects we have created a model version without biology (NoBio), in addition to the Full model described above. Model NoBio is used to determine the physical components $C_{sat,phys}$, $C_{dis,phys}$ and a model version without $CaCO_3$ cycling ($NoCaCO_3$) is used to diagnose the effect of the hard-tissue pump. The biological preformed components $C_{sat,bio} = C_{sat} - C_{sat,phys}$ and $C_{dis,bio} = C_{dis} - C_{dis,phys}$ are calculated as differences from the full model, which has been shown to be a good approximation [14].

3. Experiments

After a 7,000-year spin-up to equilibrium with prescribed pre-industrial forcing, including CO_2 and $\delta^{13}C_{CO2}$, the model was run for 5,000 years with prognostic (variable) CO_2, which reaches 278 ppm (Table 1), in good agreement with preindustrial ice core observations [45]. At this point, the same LGM boundary conditions as in Muglia et al. [41] were applied instantaneously: increased soluble iron fluxes in the Southern Ocean, reduced sedimentary iron fluxes due to lower sea level, increased salinity, prescribed ice sheets and radiative forcing from methane and nitrous oxide, prescribed wind stress anomalies and decreased meridional moisture fluxes in the Southern Hemisphere. The latter causes an AMOC shoaling, which leads to a good agreement with $\delta^{13}C_{cib}$ and radiocarbon data from LGM ocean sediments [43]. This state has also been used in K19. Although, atmospheric CO_2 was allowed to vary, $\delta^{13}C_{CO2}$ = -6.5 ‰ was kept fixed, consistent with ice core measurements [46]. Imposition of prescribed ice sheets affects terrestrial carbon storage, which instantaneously decreases by ~400 Pg (in exp $NoCaCO_3$ only by ~360 Pg; Table 1), because of the loss of vegetation and soil carbon where the ice was added. This can be thought of as land carbon buried by the ice [47], but it is unclear how much carbon was permanently buried and how much was transported by ice movement to the margins, where it could have been respired and entered the atmosphere. Note that our model does not have permafrost and the expansion of land carbon into the exposed continental shelves during the LGM is not considered. Given these uncertainties, we decided to fix $\delta^{13}C_{CO2}$, which provides realistic boundary conditions for the ocean. The LGM simulations were brought to equilibrium after a 7,000-year spin-up. The results below are from 200-year-averaged analysis simulations starting at the end of the LGM and variable CO_2 PI spin-ups.

Table 1. Global carbon budget and temperatures. C_A, C_O = DIC + DOC, and C_L are the atmospheric, ocean, and land carbon contents, respectively, and $C = C_A + C_O + C_L$ is their sum. SAT is surface air temperature and T_O is whole ocean temperature.

	DIC	DOC	CO_2	C_A	C_O	C_L	C	SAT	T_O
Experiment	**(Pg)**	**(Pg)**	**(ppm)**	**(Pg)**	**(Pg)**	**(Pg)**	**(Pg)**	**(˚C)**	**(˚C)**
Full									
PI	37,338	46	278	583	37,385	1,788	39,756	13.3	3.4
LGM	37,634	43	191	400	37,678	1,276	39,354	7.6	0.9
LGM-PI	296	-3	-87	-183	293	-512	-402	-5.7	-2.5
NoBio									
PI	35,254	0	278	583	35,254	1,788	37,625	13.2	3.4
LGM	35,209	0	251	527	35,209	1,486	37,222	9.2	1.3
LGM-PI	-45	0	-27	-56	-45	-302	-403	-4.0	-2.1
$NoCaCO_3$									
PI	37,941	47	275	578	37,989	1,782	40,349	13.2	3.4
LGM	38,298	43	189	396	38,343	1,267	40,006	7.6	0.8
LGM-PI	357	-4	-86	-182	354	-515	-343	-5.6	-2.6

https://doi.org/10.1371/journal.pclm.0000434.t001

4. Results

4.1. Climate and carbon

As a result of imposing LGM boundary conditions, atmospheric CO_2 drops and eventually reaches ~190 ppm in the Full and NoCaCO$_3$ models (Table 1), consistent with ice core observations [48]. The similarity of those models indicates that changes in the $CaCO_3$ cycle play no significant role in the reduction of atmospheric CO_2 in the Full model. Global cooling of surface air temperatures by ~-5.7˚C and of whole ocean temperatures by -2.5˚C in those models is in good agreement with observation-based estimates [49–51]. However, model NoBio only cools by -4.0˚C because its atmospheric CO_2 decline is only 27 ppm and thus much less than the ~87 ppm in the models with the soft-tissue biology included. Thus, changes in soft-tissue carbon cycling reduce atmospheric pCO_2 in the full LGM model by 60 ppm. Note that this large effect of the soft-tissue pump is amplified by reducing atmospheric pCO_2 and cooling temperatures, which enhances carbon storage further, and thus is entirely consistent with a total effect of temperature causing 45 ppm of the LGM-PI pCO_2 changes in K19.

The land carbon inventory decreases in the full model by 512 Pg, which includes 400 Pg buried by ice plus 110 Pg reduction simulated by the land model outside of ice covered areas. This implies that its atmospheric CO_2 decrease is due to the 293 Pg increase in ocean carbon (C_O = DIC + DOC), which is almost exclusively driven by DIC. The increase by 309 Pg in the sum of the components of the carbon decomposition reproduces the total DIC increase within 5% accuracy (x symbols in Fig 2C). Although the absolute DIC inventories of the PI and LGM runs are overestimated by ~100 Pg they are reproduced within 0.3% accuracy (x symbols in Fig 2A). We conclude that the errors of the decomposition are small enough to allow an accurate and complete assessment of the simulated changes in total DIC. A more detailed error analysis is presented in Section F in S1 Text.

4.2. Ocean carbon components

We decompose DIC = C_{pre} + C_{reg} into preformed and regenerated components. The preformed component C_{pre} = C_{sat} + C_{dis} consists of saturation C_{sat} = $C_{sat,phys}$ + $C_{sat,bio}$ and disequilibrium C_{dis} = $C_{dis,phys}$ + $C_{dis,bio}$ carbon, both of which are separated into physical and biological contributions. Regenerated carbon C_{reg} = C_{soft} + C_{CaCO3} results from the accumulation of respired soft-tissue carbon and dissolved calcium carbonate. Thus, total DIC = $C_{sat,phys}$ + $C_{sat,bio}$ + $C_{dis,phys}$ + $C_{dis,bio}$ + C_{soft} + C_{CaCO3} = C_{phys} + C_{bio} can also be written as the sum of physical C_{phys} = $C_{sat,phys}$ + $C_{dis,phys}$ and biological C_{bio} = $C_{sat,bio}$ + $C_{dis,bio}$ + C_{soft} + C_{CaCO3} processes. Biological carbon storage can be regarded as the direct or active part of the biological pump (C_{reg} = C_{soft} + C_{CaCO3}) plus contributions from biology on preformed carbon $C_{pre,bio}$ = $C_{sat,bio}$ + $C_{dis,bio}$.

The carbon components and their changes, shown in Figs 2A, 2C, 3A, 3C, 4A, 4C and 4E, and Section G in S1 Text, are very similar to those of K19. For this reason, they will not be discussed in detail here. Instead, we will only present a summary except for significant differences with that study. The model's PI DIC inventory is with 37,348 Pg close to, but slightly larger, than that estimated by DeVries [1; 37,100 Pg]. Simulated PI DIC concentrations at the surface and in the deep ocean are in good agreement with observations (Figs 3A and 4A). The bulk of the model's DIC storage is due to physical saturation $C_{sat,phys}$ = 36,025 Pg (Table 2). However, the actual DIC storage in model NoBio (C_{phys} = $C_{sat,phys}$ + $C_{dis,phys}$) is 761 Pg lower ($C_{dis,phys}$ = -761 Pg). The physical disequilibrium is negative mainly because surface waters flowing south in the Southern Ocean lose heat to the atmosphere, which increases their solubility (Fig 1A), but slow ingassing from the atmosphere prevents equilibration to be reached before waters

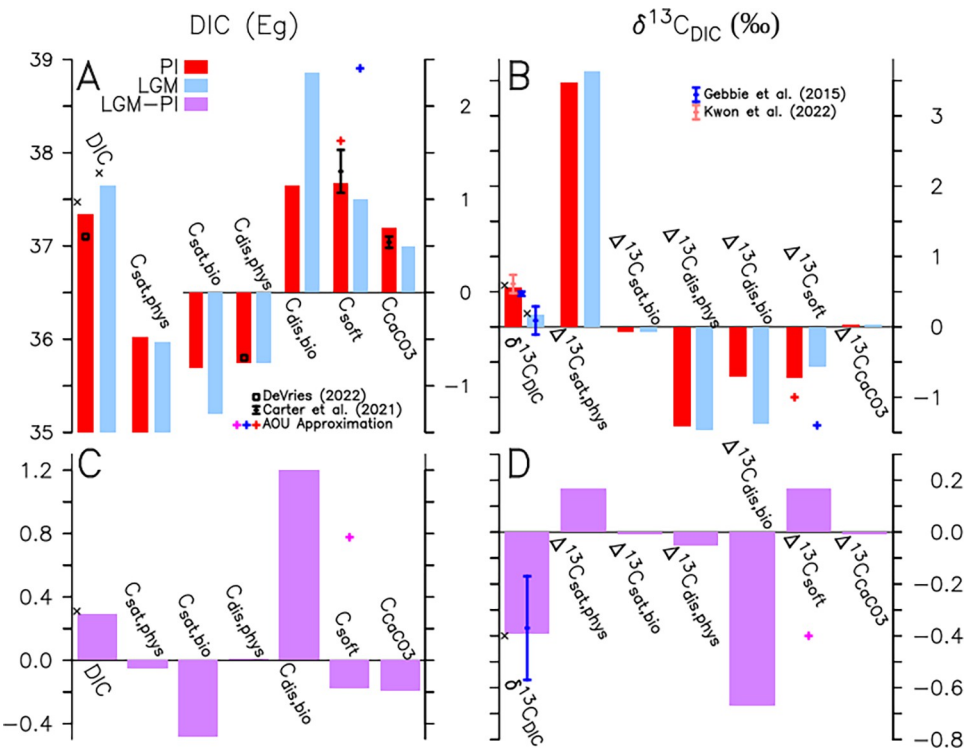

Fig 2. Components of global ocean C (panel A, C) in units of Exagram (1Eg = 10^{18}g = 1,000 Pg) and $\delta^{13}C$ (panels B, D) in units of permille. Panels A & B show absolute values from the PI (red colums) and LGM (blue columns). Panels C & D show LGM-PI differences. In panel A, the left axis applies to DIC and $C_{sat,phys}$, whereas the right axis applies to the other components. X-symbols in the leftmost columns indicate the sum of the individual components; compared to the total, they indicate the accuracy of the method. Plus-symbols represent AOU approximations. Other symbols indicate observation-based estimates [1,52–54]. We have corrected the LGM-PI change in $\delta^{13}C_{DIC}$ from [52] (-0.32 ‰) by subtracting 0.05 ‰ due to a decrease in global mean [CO_3] by 20.5 μmol/kg in the model using the regression slope of -0.0026 ‰/(μmol/kg) estimated by [34].

https://doi.org/10.1371/journal.pclm.0000434.g002

subduct and sink to the deep ocean [14]. Thus, the deep ocean's carbon storage is less than it would be at equilibrium. Our estimate of $C_{dis,phys}$ is in good agreement with that of DeVries [1; -700 Pg].

$C_{sat,phys}$ and $C_{dis,phys}$ do not change much in the LGM. $C_{sat,phys}$ is determined by the surface DIC(T, S, pCO_{2o}, ALK) concentration in NoBio. At equilibrium, the ocean pCO_2 (pCO_{2o}) is equal to that of the atmosphere (pCO_{2a}). Thus, $C_{sat,phys}$ depends on temperature T and pCO_{2a}, both of which changed considerably in the LGM. Effects of salinity (S) and alkalinity (ALK) changes in NoBio are minor. However, cooler temperatures would have increased $C_{sat,phys}$,

Table 2. Global Components for C (Pg) and $\Delta^{13}C$ (‰).

	$C_{sat,phys}$	$C_{sat,bio}$	$C_{dis,phys}$	$C_{dis,bio}$	C_{soft}	C_{CaCO3}	C_{phys}	C_{bio}
PI	36,025	-812	-761	1,155	1,175	690	35,264	2,208
LGM	35,971	-1,297	-752	2,360	999	501	35,219	2,562
LGM-PI	-54	-485	9	1,205	-176	-189	-45	355
	$\Delta^{13}C_{sat,phys}$	$\Delta^{13}C_{sat,bio}$	$\Delta^{13}C_{dis,phys}$	$\Delta^{13}C_{dis,bio}$	$\Delta^{13}C_{soft}$	$\Delta^{13}C_{CaCO3}$	$\Delta^{13}C_{phys}$	$\Delta^{13}C_{bio}$
PI	3.47	-0.07	-1.42	-0.70	-0.73	0.04	2.04	-1.46
LGM	3.64	-0.08	-1.48	-1.37	-0.56	0.03	2.16	-1.98
LGM-PI	0.17	-0.01	-0.05	-0.67	0.16	-0.01	0.12	-0.52

https://doi.org/10.1371/journal.pclm.0000434.t002

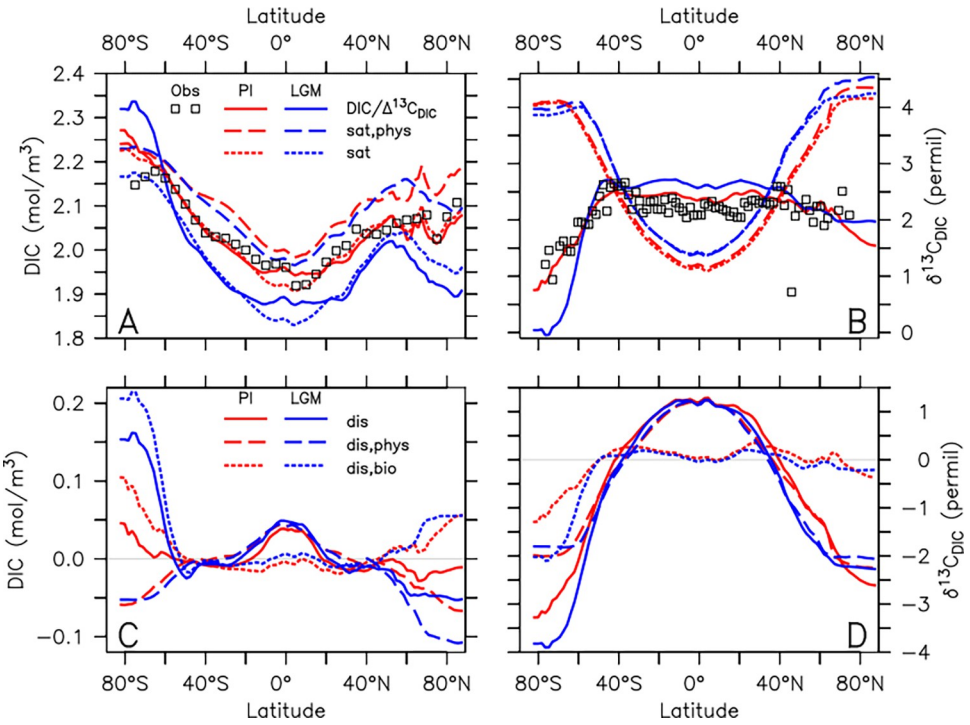

Fig 3. Zonally averaged surface values of DIC concentrations (left) and $\delta^{13}C_{DIC}$ (right) and their decompositions for the PI (red) and the LGM (blue). Observations (square symbols) of PI DIC and $\delta^{13}C_{DIC}$ are from (A) GLODAP2.2021 [55,56] and (B) Kwon et al. [54], respectively, corrected for anthropogenic carbon. Legend in panels (A) and (C) also apply to panels (B) and (D), respectively.

https://doi.org/10.1371/journal.pclm.0000434.g003

while lower pCO_{2a} would have decreased it, resulting in a small net effect. Overall, DIC in NoBio's LGM simulation decreased by 45 Pg compared to the PI, which together with the loss of 56 Pg from the atmosphere (27 ppm) is compensated by an increase in land carbon by ~100 Pg (after the burial of 400 Pg by ice; Table 1).

In the PI control run, biological saturation carbon storage $C_{sat,bio} = C_{sat} - C_{sat,phys}$ = -812 Pg is negative due to the effect of biology on alkalinity. Biological production of $CaCO_3$ reduces alkalinity at the surface. Since pCO_{2a} is identical in the PI simulations of models Full and NoBio, surface DIC equilibrium concentrations must be lower in the Full model compared with NoBio and hence $C_{sat,bio} < 0$. The spatial distribution of $C_{sat,bio}$ at the surface features large negative concentrations in the tropics, particularly in the Indian ocean, and in the North Atlantic (Fig I panel A in S1 Text). It is strongly correlated with the effect of biology on alkalinity because T, S, pCO_{2a} and the circulation are all identical between the Full model and NoBio. From the surface, large negative concentrations (-80 to -100 mol/m^3) of $C_{sat,bio}$ are advected into the mid-depth North Atlantic (Fig I panel D in S1 Text), whereas bottom waters in all ocean basins have less negative concentrations (~-40 mol/m^3; Fig I panels D,G in S1 Text). In the LGM, $C_{sat,bio}$ = -1,297 Pg becomes 485 Pg more negative than in the PI (Fig 2C). This reduction is affected by changes in the pCO_{2a} and T differences between the Full model and NoBio. Since LGM pCO_{2a} is lower in the Full model than in NoBio, surface DIC at saturation in the Full model will be reduced more than in NoBio ($\Delta C_{sat} = C_{sat,LGM} = C_{sat,PI} < \Delta C_{sat,phys} = C_{sat,phys,LGM} = C_{sat,phys,PI}$). $CaCO_3$ cycling decreases $C_{sat,bio}$ by 1,051 Pg in PI and by 801 Pg in the LGM (Full–$NoCaCO_3$).

As in K19, the largest driver of the increase in ocean carbon storage is the biological disequilibrium $C_{dis,bio}$. It approximately doubles from 1,155 Pg in the PI to 2,360 Pg in the LGM.

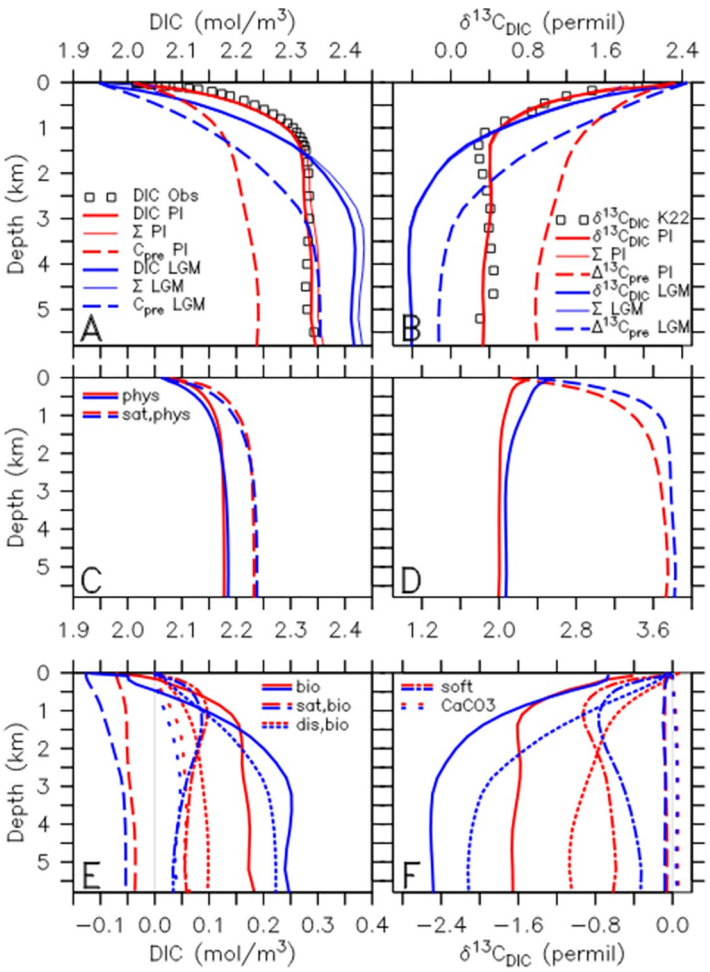

Fig 4. Horizontally averaged profiles of DIC (left) and $\delta^{13}C_{DIC}$ (right) and their decomposition in the PI (red) and LGM (blue) runs. Top panels show DIC (thick solid) and C_{pre} (dashed). The difference is C_{reg} = DIC–C_{pre}. Thin lines show the sum of the components for comparison with DIC. Observations (square symbols) are from GLODAP2.2021 [55,56] and Kwon et al. [54] corrected for anthropogenic carbon. Panels C & D show physical components C_{phys} and $\Delta^{13}C_{phys}$ (solid), and $C_{sat,phys}$ and $\Delta^{13}C_{sat,phys}$ (dashed), respectively. The difference is the physical disequilibrium e.g. $C_{dis,phys} = C_{sat,phys} - C_{phys}$. Panels E & F show the biological components.

https://doi.org/10.1371/journal.pclm.0000434.g004

It is likely that, as in K19, sea ice, iron fertilization, and circulation changes all conspire to force the large increase in $C_{dis,bio}$ in the LGM simulation. Our estimate of $C_{dis,bio}$ in the PI is larger than that from a recent study using a data-assimilated model including the soft-tissue pump only [33; 487 Pg]. However, this discrepancy is not due to the presence of the $CaCO_3$ cycle in our model. In model NoCaCO$_3$ $C_{dis,bio}$ is 1,244 Pg, slightly higher than in the Full model. The large difference between our model and that of Nowicki et al. is disconcerting and should be investigated further but is beyond the scope of this work.

Regenerated components C_{soft} = 1,175 Pg and C_{CaCO3} = 690 Pg in our PI model are in good agreement with estimates by Carter et al. [53; 1,300+-230 and 540+-60 Pg, respectively]. Both components decrease in the LGM by 180–190 Pg, consistent with decreased export production, as in K19. Even though enhanced iron fertilization in the Southern Ocean forces C_{soft} to increase, reduced meridional overturning circulation and increased sea ice cover decrease productivity and hence C_{soft} through increased nutrient and light limitation of phytoplankton

growth (K19). However, despite reduced C_{reg} and $C_{sat,bio}$ biological carbon storage as a whole C_{bio} increases by 355 Pg in the LGM, due to the large increase in $C_{dis,bio}$.

4.3. Ocean carbon-13 components

The decomposition of $DI^{13}C$ is analogous to that of DIC. Expressing the components in delta notation $\delta^{13}C_{DIC} = \Delta^{13}C_{pre} + \Delta^{13}C_{reg}$, we use capital delta (Δ) to refer to weighted-average, additive components (Section A in S1 Text), where preformed contributions $\Delta^{13}C_{pre} = \Delta^{13}C_{sat} + \Delta^{13}C_{dis} = \Delta^{13}C_{sat,phys} + \Delta^{13}C_{sat,bio} + \Delta^{13}C_{dis,phys} + \Delta^{13}C_{dis,bio}$ are the sum of saturation and disequilibrium components and regenerated components $\Delta^{13}C_{reg} = \Delta^{13}C_{soft} + \Delta^{13}C_{CaCO3}$ include contributions from soft and hard tissue pumps, although the latter are negligible as will be shown below.

Whole ocean $\delta^{13}C_{DIC}$ (Fig 1) is 0.58 ‰ in the PI and 0.18 ‰ in the LGM, in good agreement with observation-based estimates [22,52,54]. Note that the LGM-PI estimate of -0.32 ‰ from [52], mentioned earlier, was not corrected for the effect of carbonate ion changes. Doing so, using the modeled carbonate ion change yields -0.37 ‰, in excellent agreement with our model estimate of -0.39 ‰. The sum of the components in our decomposition precisely reproduces this value as well as the absolute values in the PI and LGM, even though locally small differences occur (Section F in S1 Text). The spatial distribution of $\delta^{13}C_{DIC}$ in both PI and LGM simulations is also in good agreement with observations (Figs 3B, 4B and 5A). The PI features high values (2–2.5 ‰) near the surface, except near Antarctica where they drop to ~1 ‰, and lower values at depth (~0.5 ‰). The model also reproduces the PI interbasin differences with relatively high values (~1 ‰) in the deep Atlantic and lower values (~0 ‰) in the deep Pacific (Fig 5D and 5G, Fig B in S1 Text).

A striking long-known feature of the LGM distribution in Atlantic sediment reconstructions is the increased vertical gradient at mid depths [57,58], which the model reproduces, although it somewhat overestimates it. In the model, this steepened gradient is due to enhanced iron fertilization in the Southern Ocean, which increases productivity there and injects more isotopically light carbon in deep waters, a shoaling of the Atlantic Meridional Overturning Circulation (AMOC), which shifts the southward penetration of relatively isotopically high North Atlantic Deep Water to shallower depths and an increase in sea ice cover, which prevents equilibration with the atmosphere. The decrease in observed deep Atlantic $\delta^{13}C_{DIC}$ by about 1 ‰ is well reproduced by the model (Fig 5B), although it extends to slightly shallower depths. This may be due to a too shallow and weak simulated AMOC (Fig E in S1 Text). The decrease in the deep Southern Ocean is slightly underestimated, while that in the Indian and Pacific is slightly overestimated by the model (Fig 5E and 5H). Nevertheless, we conclude that the model captures the main features in the sediment data and thus is a viable representation of the LGM state that justifies further analysis. One caveat of this model state is hypoxic conditions in the northern North Pacific, which are inconsistent with sediment data. These biases suggest more carbon and less oxygen in the North Pacific and less carbon and more oxygen in the Southern Ocean in the model compared to the reconstructions.

Figs 2D, 4F, 5C, 5F and 5I reveal that $\Delta^{13}C_{dis,bio}$ is by far the dominating term in the $\delta^{13}C_{DIC}$ decrease. Globally, it amounts to -0.67 ‰ (Table 2) and in the deep ocean it decreases $\delta^{13}C_{DIC}$ by about 1 ‰. The fact that deep ocean $\delta^{13}C_{DIC}$ decreases less than that is owed to positive changes in $\Delta^{13}C_{sat,phys}$ and $\Delta^{13}C_{soft}$ by 0.2–0.3 ‰ (Fig 4D and 4F). Globally, each of those components increases $\delta^{13}C_{DIC}$ by 0.16–0.17 ‰ (Table 2).

The spatial distribution of $\Delta^{13}C_{dis,bio}$, shown in Fig 6 reveals that it is dominated by the Southern Ocean. In the PI, minimum values of $\Delta^{13}C_{dis,bio}$ of ~-1.2 ‰ are simulated in the marginal polar seas, which propagate as AABW into the abyssal waters of all ocean basins. In the

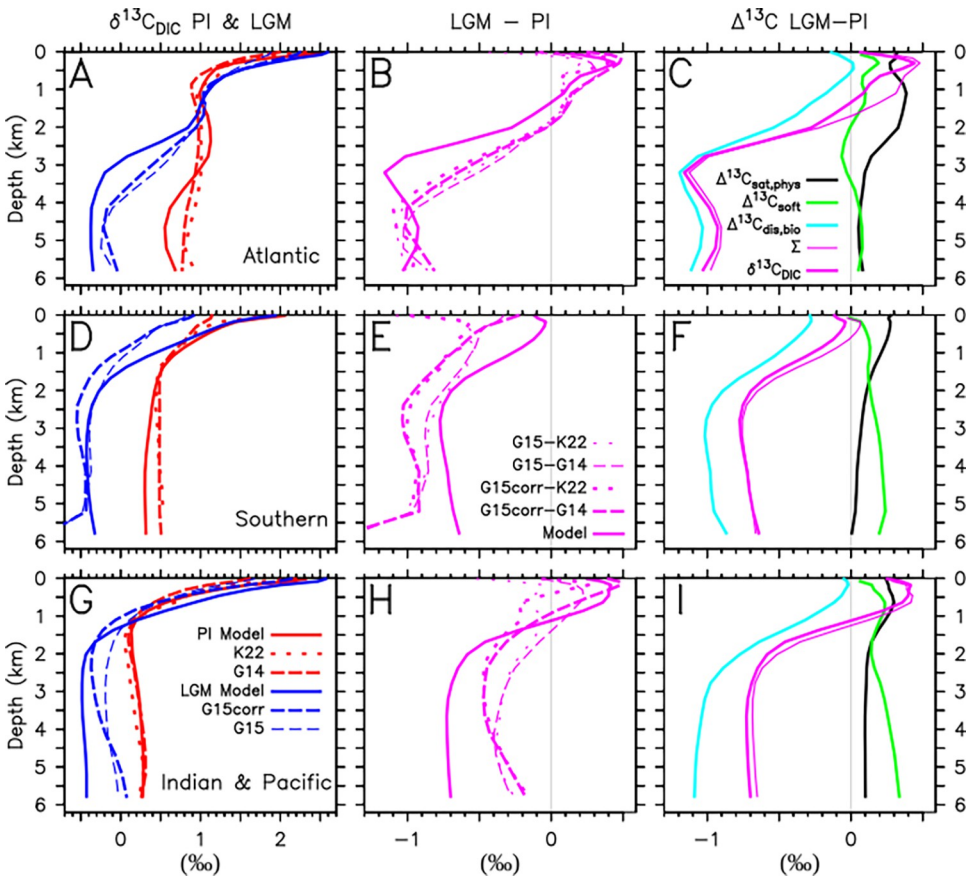

Fig 5. Horizontally-averaged profiles of $\delta^{13}C_{DIC}$ and its decomposition in the Atlantic (A,B,C), Southern Ocean (south of 40˚S; D,E,F), and Pacific and Indian (G,H,I). Panels A,D&G show absolute values for the PI (red) and LGM (blue). Thick solid lines are model results. Observation-based estimates are shown as thick red dotted [54], tick red dashed [22], thick blue dashed [52] corrected according to calibration LA1 of Schmittner et al. [34], and thin blue dashed line are the uncorrected data from [52]. Panels B,E&H show LGM-PI differences. Panels C,F&I show the three dominant terms in the $\delta^{13}C_{DIC}$ decomposition for the LGM-PI. The thick solid purple line is the same as in panels B, E&H. The thin purple line is the sum of the three components ($\Delta^{13}C_{sat,phys}$, $\Delta^{13}C_{soft}$, $\Delta^{13}C_{dis,bio}$).

https://doi.org/10.1371/journal.pclm.0000434.g005

LGM, values twice as large (~-2.4 ‰) extend more spatially at the surface around Antarctica and penetrate not only abyssal waters but also much of the mid depth oceans. The LGM-PI changes in $\Delta^{13}C_{dis,bio}$ (Fig 6F) feature a minimum in the North Atlantic around 3.5 km depth, due to AMOC shoaling.

4.4. Approximations

The AOU approximation of carbon storage due to the soft-tissue biological pump $C_{soft,AOU} = r_{C:O} \cdot AOU$, where $AOU = O_2 - O_{2,sat}$ is the Apparent Oxygen Utilization and $r_{C:O} = 0.64$ is the carbon to oxygen ratio, is popular both in models and observations if oxygen concentrations are available. In the PI (Fig 2A), the AOU approximation $C_{soft,AOU}$ = 1,628 Pg, overestimates C_{soft} by 43%, consistent with previous results [2,26,27]. Since oxygen is substantially undersaturated in surface waters around Antarctica that fill much of the deepest ocean layers, AOU is positive there, whereas true oxygen utilization and C_{soft} are both zero at the surface. Propagation of that positive excess AOU signal into the ocean interior leads to the large error of this approximation. It may be argued that the AOU approximation includes the biological

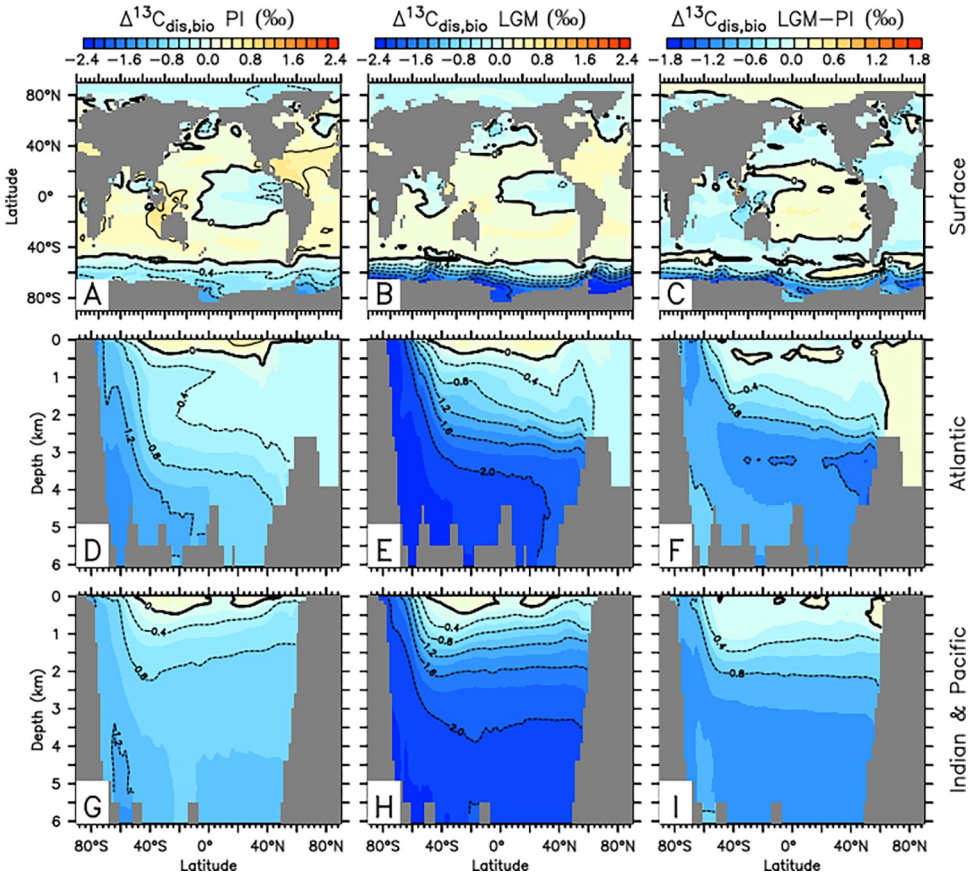

Fig 6. Modelled distribution of $\Delta^{13}C_{dis,bio}$ (‰) in the PI (A,D,G), LGM (B,E,H) and the difference (LGM-PI; C,F,I) at the surface (A,B,C) and zonally-averaged in the Atlantic (D,E,F) and Pacific and Indian (G,H,I).

https://doi.org/10.1371/journal.pclm.0000434.g006

disequilibrium. However, $C_{soft} + C_{dis,bio}$ = 2,330 Pg, thus the AOU approximation underestimates that quantity by 30%. This makes sense because the oxygen disequilibrium is generally smaller than that of carbon. But one cannot be inferred from the other. In the LGM, the AOU approximation errors become even larger, $C_{soft,AOU}$ = 2,405 Pg, overestimating C_{soft} by a factor of 2.4. As in K19, the AOU approximation leads to the wrong sign of the LGM-PI changes (Fig 2C): $\Delta C_{soft,AOU}$ = +777 Pg, whereas the precise calculation yields ΔC_{soft} = -176 Pg, thus a factor of -4.4 error.

For the isotopes, the AOU approximation $\Delta^{13}C_{soft,AOU} = AOU\cdot(-1.1)/170$ [24] is similarly erroneous. In the PI, $\Delta^{13}C_{soft,AOU,PI}$ = -1.02 ‰, which overestimates the magnitude of the precise value $\Delta^{13}C_{soft,PI}$ = -0.73 ‰ by 40%, whereas in the LGM $\Delta^{13}C_{soft,AOU,LGM}$ = -1.50 ‰, thus overestimating $\Delta^{13}C_{soft,LGM}$ = -0.56 ‰ by a factor of 2.7 (Fig 2B). Similar to carbon, the AOU approximation gives a wrong sign of the LGM-PI changes in the isotopic composition $\Delta^{13}C_{soft,AOU,LGM}-\Delta^{13}C_{soft,AOU,PI}$ = -0.49 ‰ vs $\Delta^{13}C_{soft,LGM}-\Delta^{13}C_{soft,PI}$ = +0.16 ‰, demonstrating the unreliability of the AOU approximation (Fig 2D).

The popular air-sea approximation $\delta^{13}C_{as} = \delta^{13}C_{DIC}-(2.7–1.1\times PO_4)$, which can be used in models and observations when phosphate estimates are available, does not perform better. Since $\delta^{13}C_{as}$ aims to remove the effects of biology [10,15], the conceptually most related quantity in our decomposition is $\Delta^{13}C_{phys}$, although it may be argued that it should be compared to $\Delta^{13}C_{pre} = \delta^{13}CDIC-\Delta^{13}C_{reg}$, if the phosphate relation represents regenerated carbon only. In the PI, $\delta^{13}C_{as,PI}$ = 0.28 ‰, whereas $\Delta^{13}C_{phys,PI}$ = 2.04 ‰ and $\Delta^{13}C_{pre,PI}$ = 1.27 ‰, thus $\delta^{13}C_{as}$ is

not a good approximation for either. This conclusion is confirmed for the LGM, $\delta^{13}C_{as,LGM}$ = -0.11 ‰, whereas $\Delta^{13}C_{phys,LGM} = \Delta^{13}C_{pre,LGM}$ = 2.16 ‰. The LGM-PI changes are $\delta^{13}C_{as,LGM}$—$\delta^{13}C_{as,PI}$ = -0.39 ‰, whereas $\Delta^{13}C_{phys,LGM}$—$\Delta^{13}C_{phys,PI}$ = 0.12 ‰ and $\Delta^{13}C_{pre,LGM}$—$\Delta^{13}C_{pre,PI}$ = -0.55 ‰. We conclude that $\delta^{13}C_{as}$ does not approximate any of those quantities or their changes well.

It is clear that $\delta^{13}C_{as}$ does not remove all effects of biology on $\delta^{13}C_{DIC}$. If it did, its changes in the LGM would have a positive sign since cooling increases $\delta^{13}C_{DIC}$, mainly through $\Delta^{13}C_{sat,phys}$ (Fig 2B; Table 2). But $\delta^{13}C_{as}$ doesn't approximate $\Delta^{13}C_{pre}$ well either, because it includes preformed phosphate, which does not undergo air-sea gas exchange and thus its changes are different from those of preformed $\delta^{13}C_{DIC}$ [59].

5. Discussion and conclusions

We have demonstrated that widely used approximations of respired carbon and $\delta^{13}C_{DIC}$, based on the AOU approximation or phosphate ($\delta^{13}C_{as}$) lead to large errors, in this case even wrong signs, and thus should not be used anymore. They confuse air-sea disequilibrium of oxygen with that of carbon and preformed phosphate with that of $\delta^{13}C_{DIC}$, which makes them invalid. Conclusions based on those approximations need to be re-evaluated. For example, the conclusion of Sigman and Hain [3], that the changes in preformed $\delta^{13}C_{DIC}$ in the LGM were zero, thus implying that the observed whole ocean decrease in $\delta^{13}C_{DIC}$ was due to respired carbon indicating an increased biological pump, was based on the AOU approximation of $\Delta^{13}C_{soft}$ by Vollmer et al. [24]. In contrast, here we find that the whole ocean decrease in $\delta^{13}C_{DIC}$ of -0.39 ‰ was caused by a large decrease in preformed $\Delta^{13}C_{pre}$ of -0.55 ‰, dominated by the biological disequilibrium $\Delta^{13}C_{dis,bio}$ change of -0.67 ‰.

The soft-tissue biological pump is driven by the sinking flux of organic matter, which is isotopically light and leads to depletion of surface DIC and enrichment of $\delta^{13}C_{DIC}$ (Fig 1A), resulting in uptake of CO_2 from the atmosphere at mid and low latitudes and a tendency of air-sea fluxes to decrease $\delta^{13}C_{DIC}$ there. In the subsurface ocean, the remineralization of the organic matter increases DIC and decreases $\delta^{13}C_{DIC}$. Thus, $C_{soft} > 0$ and $\Delta^{13}C_{soft} < 0$. In other words, the sinking flux of organic matter is a source for biological carbon and a sink for $\delta^{13}C_{DIC}$. If this was the only process operating, ocean carbon would increase, and its $\delta^{13}C_{DIC}$ would decrease, indefinitely. This is obviously not the case. At equilibrium, this source for biological carbon has an equal sink in upwelling and outgassing of C_{bio} to the atmosphere, which increases $\delta^{13}C_{DIC}$. If air-sea gas exchange was infinitely fast, the disequilibrium would be zero. However, since gas exchange is slow, a disequilibrium $C_{dis,bio} > 0$ and $\Delta^{13}C_{dis,bio} < 0$ remains near Antarctica (Fig 3C and 3D), which fills the deepest layers of the ocean (Fig 6).

Physical processes, in contrast, lead to cooling at the surface, which causes negative disequilibria ($C_{dis,phys} < 0$ and $\Delta^{13}C_{dis,bio} < 0$) and surface fluxes in the polar Southern Ocean overturning circulation branch that tend to increase both CO_2 and $\delta^{13}C_{DIC}$ (Fig 1A). Thus, while for carbon the biological and physical disequilibria oppose and diminish each other, for $\delta^{13}C_{DIC}$ they collaborate and strengthen one another (Fig 2). This leads to a much larger effect of the disequilibrium for $\delta^{13}C_{DIC}$ than for carbon.

Two processes affect biological carbon storage. First, the active biological pump, the source of biological carbon, which transports carbon against a gradient in analogy to Volk and Hoffert's [11] cellular ion pump, associated with photosynthesis, sinking of organic matter and accumulation of regenerated carbon at depth, quantified as C_{reg}. Second, the sink of biological carbon associated with upwelling and outgassing, which, because it is ineffective, especially near Antarctica, leaves a substantial disequilibrium ($C_{dis,bio}$, $\Delta^{13}C_{dis,bio}$), thus adding to the storage of isotopically light biological carbon. It is useful to distinguish between these because

regenerated carbon is impacted by processes that affect productivity such as nutrient or light limitation and the residence time of waters in the subsurface, whereas the disequilibrium is impacted by processes that affect gas exchange such as sea ice and the proportion of the deep ocean that is ventilated from Antarctic polar waters. Even though biological carbon increased in our LGM simulations, the active part of the biological pump decreased (C_{reg}), which leads to an increase in $\Delta^{13}C_{reg}$. Instead, we attribute the increase in biological carbon storage and decrease in $\Delta^{13}C_{bio}$ to changes in the biological disequilibrium, representing a diminished sink of biological carbon.

Shackleton's [35] hypothesis, that a reduction in terrestrial carbon would have caused the whole ocean decrease in $\delta^{13}C_{DIC}$, implies that $\Delta^{13}C_{sat}$ is the dominant term in our model's decomposition. However, that is not the case. Rather, our results suggest that processes that affect the biological disequilibrium are the main drivers of the observed decrease in $\delta^{13}C_{DIC}$, such as increased sea ice cover, iron fertilization and shoaling of the AMOC. However, here we have not performed single forcing experiments such as in K19. Therefore, a quantification of each forcing variable on the simulated changes in the carbon isotope components will need to wait until further study. Nevertheless, another argument against Shackleton's hypothesis and studies that support that idea [36,37], is that it assumes a closed land-ocean-atmosphere system in which carbon and carbon-13 are conserved. However, ample evidence suggests that sediment interactions played a role on glacial-interglacial timescales [60,61], and that they have affected both carbon and $\delta^{13}C$ [62]. Thus, estimates of terrestrial carbon changes from whole ocean $\delta^{13}C_{DIC}$ based on the assumption of a closed system are likely flawed.

Our simulations also assume a closed system. Sediment interactions, specifically the dissolution of calcium carbonate, would have increased ocean carbon and alkalinity, more than in our model, and further reduced atmospheric CO_2. This effect could have compensated for the respiration of some or all the terrestrial carbon that was buried under ice in our simulations. However, the effect of the dissolution of ~970 Pg of calcium carbonate with a $\delta^{13}C$ of 1.5 ‰ [38] would have increased whole ocean $\delta^{13}C_{DIC}$ by only ~0.04 ‰, a relatively small effect, and thus does not affect our estimated $\delta^{13}C_{DIC}$ decomposition much. Nevertheless, simulations with a more complete carbon cycle, including sediments, permafrost and sea level are desirable.

Supporting information

S1 Text. Supplementary text. Fig A in S1 Text: Horizontally averaged (left columns) and zonal average simulated DIC distribution compared to observations [63]. Fig B in S1 Text: Horizontally averaged (left columns) and zonal average simulated $\delta^{13}C$ of DIC distribution compared to observations [20]. Fig C in S1 Text: Horizontally averaged (left columns) and zonal average simulated PO_4 distribution compared to observations [64]. Fig D in S1 Text: Meridional Overturning Circulation in the PI. Top: world ocean, center: Atlantic, bottom: Indian & Pacific. Eulerian streamfunction is shown in Sv (1 Sv = 10^6 m^3/s). Positive values (solid lines) represent clockwise flow, negative (dashed) counterclockwise. Fig E in S1 Text: As S4 Fig but for the LGM. Fig F in S1 Text: Errors induced by the decomposition in DIC (A, B) and $\delta^{13}C$ of DIC (C, D) in the PI simulation. Panels A and C are horizontally averaged, while B and D are zonal averages, where Sum = $C_{pref} + C_{soft} + C_{CaCO3}$. Fig G in S1 Text: Errors induced by the decomposition in DIC (A, B) and $\delta^{13}C$ of DIC (C, D) in the LGM simulation. Panels A and C are horizontally averaged, while B and D are zonal averages, where Sum = $C_{pref} + C_{soft} + C_{CaCO3}$. Fig H in S1 Text: Modelled distribution of $C_{sat,phys}$ ($mmol/m^3$) in the PI (A,D,G), LGM (B,E,H) and the difference (LGM-PI; C,F,I) at the surface (A,B,C) and zonally-averaged in the Atlantic (D,E,F) and Pacific and Indian (G,H,I). Contour lines in A-C are sea surface

temperatures. Fig I in S1 Text: As Fig H in S1 Text, but for $C_{sat,bio}$. Contour lines in (A) show the effects of biology on alkalinity (difference in alkalinity between the full model and model NoBio). Fig J in S1 Text: As Fig H in S1 Text, but for $C_{dis,phys}$. Contour lines are also $C_{dis,phys}$. Fig K in S1 Text: As Fig H in S1 Text, but for $C_{dis,bio}$. Fig L in S1 Text: As Fig H in S1 Text, but for C_{soft}. Top row shows maps at 700 m depth. Fig M in S1 Text: As Fig H in S1 Text, but for C_{CaCO3}. Top row shows maps at 4,000 m depth. Note the different color scales compared with S8 Fig. Fig N in S1 Text: As Fig 6 in the main text, but for $\Delta^{13}C_{sat,phys}$. Contour lines are potential temperature. Fig O in S1 Text: As Fig 6 in the main text, but for $\Delta^{13}C_{sat,bio}$. Fig P in S1 Text: As Fig 6 in the main text, but for $\Delta^{13}C_{dis,phys}$. Contour lines are $\Delta^{13}C_{dis,phys}$. Fig Q in S1 Text: As Fig 6 in the main text, but for $\Delta^{13}C_{soft}$. Contour lines are $\Delta^{13}C_{soft}$. Fig R in S1 Text: As Fig 6 in the main text, but for $\Delta^{13}C_{CaCO3}$. Contour lines are $\Delta^{13}C_{CaCO3}$.
(PDF)

Acknowledgments

We thank Samar Khatiwala for contributing ideas to calculate $^{13}C_{sat}$ as described in Section C in S1 Text. We are grateful for constructive reviews from Michel Crucifix and one anonymous reviewer.

Author Contributions

Conceptualization: Andreas Schmittner.

Formal analysis: Andreas Schmittner, Nathaniel J. Fillman.

Funding acquisition: Andreas Schmittner.

Investigation: Andreas Schmittner, Nathaniel J. Fillman.

Methodology: Andreas Schmittner, Nathaniel J. Fillman.

Project administration: Andreas Schmittner.

Software: Nathaniel J. Fillman.

Supervision: Andreas Schmittner.

Validation: Andreas Schmittner, Nathaniel J. Fillman.

Visualization: Andreas Schmittner, Nathaniel J. Fillman.

Writing – original draft: Andreas Schmittner, Nathaniel J. Fillman.

Writing – review & editing: Andreas Schmittner, Nathaniel J. Fillman.

References

1. DeVries T. The Ocean Carbon Cycle. Annual Review of Environment and Resources. 2022; 47: 317–341. https://doi.org/10.1146/annurev-environ-120920-111307
2. Khatiwala S, Schmittner A, Muglia J. Air-sea disequilibrium enhances ocean carbon storage during glacial periods. Science Advances. 2019; 5: eaaw4981. https://doi.org/10.1126/sciadv.aaw4981 PMID: 31206024
3. Sigman DM, Hain MP. Ocean Oxygen, Preformed Nutrients, and the Cause of the Lower Carbon Dioxide Concentration in the Atmosphere of the Last Glacial Maximum. Paleoceanography and Paleoclimatology. 2024; 39: e2023PA004775. https://doi.org/10.1029/2023PA004775
4. Mackensen A, Schmiedl G. Stable carbon isotopes in paleoceanography: atmosphere, oceans, and sediments. Earth-Science Reviews. 2019; 197: 102893. https://doi.org/10.1016/j.earscirev.2019.102893

5. Broecker WS, Peng T-H. Gas exchange rates between air and sea. Tellus. 1974; 26: 21–35. https://doi.org/10.3402/tellusa.v26i1-2.9733
6. Wanninkhof R. Relationship between wind speed and gas exchange over the ocean revisited. Limnology and Oceanography: Methods. 2014; 12: 351–362. https://doi.org/10.4319/lom.2014.12.351
7. Zeebe RE, Wolf-Gladrow D. CO2 in Seawater: Equilibrium, Kinetics, Isotopes. Gulf Professional Publishing; 2001.
8. Hansell DA, Carlson CA. Localized refractory dissolved organic carbon sinks in the deep ocean. Global Biogeochemical Cycles. 2013; 27: 705–710. https://doi.org/10.1002/gbc.20067
9. Zhang J, Quay PD, Wilbur DO. Carbon isotope fractionation during gas-water exchange and dissolution of CO2. Geochimica et Cosmochimica Acta. 1995; 59: 107–114. https://doi.org/10.1016/0016-7037(95)91550-D
10. Lynch-Stieglitz J, Stocker TF, Broecker WS, Fairbanks RG. The influence of air-sea exchange on the isotopic composition of oceanic carbon: Observations and modeling. Global Biogeochemical Cycles. 1995; 9: 653–665. https://doi.org/10.1029/95GB02574
11. Volk T, Hoffert MI. Ocean Carbon Pumps: Analysis of Relative Strengths and Efficiencies in Ocean-Driven Atmospheric CO2 Changes. The Carbon Cycle and Atmospheric CO2: Natural Variations Archean to Present. American Geophysical Union (AGU); 1985. pp. 99–110. https://doi.org/10.1029/GM032p0099
12. Ito T, Follows MJ. Air-sea disequilibrium of carbon dioxide enhances the biological carbon sequestration in the Southern Ocean. Global Biogeochemical Cycles. 2013; 27: 1129–1138. https://doi.org/10.1002/2013GB004682
13. Murnane RJ, Sarmiento JL. Roles of biology and gas exchange in determining the δ13C distribution in the ocean and the preindustrial gradient in atmospheric δ13C. Global Biogeochemical Cycles. 2000; 14: 389–405. https://doi.org/10.1029/1998GB001071
14. Toggweiler JR, Gnanadesikan A, Carson S, Murnane R, Sarmiento JL. Representation of the carbon cycle in box models and GCMs: 1. Solubility pump. Global Biogeochemical Cycles. 2003; 17. https://doi.org/10.1029/2001GB001401
15. Broecker WS, Maier-Reimer E. The influence of air and sea exchange on the carbon isotope distribution in the sea. Global Biogeochemical Cycles. 1992; 6: 315–320. https://doi.org/10.1029/92GB01672
16. Gruber N, Keeling CD, Bacastow RB, Guenther PR, Lueker TJ, Wahlen M, et al. Spatiotemporal patterns of carbon-13 in the global surface oceans and the oceanic suess effect. Global Biogeochemical Cycles. 1999; 13: 307–335. https://doi.org/10.1029/1999GB900019
17. Redfield AC. The processes determining the concentration of oxygen, phosphate and other organic derivatives within the depths of the Atlantic Ocean. 1942 [cited 25 Jan 2024]. Available: https://hdl.handle.net/1912/1053.
18. Gruber N, Sarmiento JL, Stocker TF. An improved method for detecting anthropogenic CO2 in the oceans. Global Biogeochemical Cycles. 1996; 10: 809–837. https://doi.org/10.1029/96GB01608
19. Kwon EY, Sarmiento JL, Toggweiler JR, DeVries T. The control of atmospheric pCO2 by ocean ventilation change: The effect of the oceanic storage of biogenic carbon. Global Biogeochemical Cycles. 2011; 25. https://doi.org/10.1029/2011GB004059
20. Schmittner A, Gruber N, Mix AC, Key RM, Tagliabue A, Westberry TK. Biology and air–sea gas exchange controls on the distribution of carbon isotope ratios (δ13C) in the ocean. Biogeosciences. 2013; 10: 5793–5816. https://doi.org/10.5194/bg-10-5793-2013
21. Williams RG, Follows MJ. Ocean Dynamics and the Carbon Cycle: Principles and Mechanisms. Cambridge University Press; 2011.
22. Gebbie G. How much did Glacial North Atlantic Water shoal? Paleoceanography. 2014; 29: 190–209. https://doi.org/10.1002/2013PA002557
23. Marchitto TM, Broecker WS. Deep water mass geometry in the glacial Atlantic Ocean: A review of constraints from the paleonutrient proxy Cd/Ca. Geochemistry, Geophysics, Geosystems. 2006; 7. https://doi.org/10.1029/2006GC001323
24. Vollmer TD, Ito T, Lynch-Stieglitz J. Proxy-Based Preformed Phosphate Estimates Point to Increased Biological Pump Efficiency as Primary Cause of Last Glacial Maximum CO2 Drawdown. Paleoceanography and Paleoclimatology. 2022; 37: e2021PA004339. https://doi.org/10.1029/2021PA004339
25. Cliff E, Khatiwala S, Schmittner A. Glacial deep ocean deoxygenation driven by biologically mediated air–sea disequilibrium. Nat Geosci. 2021; 14: 43–50. https://doi.org/10.1038/s41561-020-00667-z
26. Duteil O, Koeve W, Oschlies A, Bianchi D, Galbraith E, Kriest I, et al. A novel estimate of ocean oxygen utilisation points to a reduced rate of respiration in the ocean interior. Biogeosciences. 2013; 10: 7723–7738. https://doi.org/10.5194/bg-10-7723-2013

27. Ito T, Follows MJ, Boyle EA. Is AOU a good measure of respiration in the oceans? Geophysical Research Letters. 2004; 31. https://doi.org/10.1029/2004GL020900

28. Ito T, Follows MJ. Preformed phosphate, soft tissue pump and atmospheric CO2. Journal of Marine Research. 2005; 63: 813–839. https://doi.org/10.1357/0022240054663231

29. Galbraith ED, Martiny AC. A simple nutrient-dependence mechanism for predicting the stoichiometry of marine ecosystems. Proceedings of the National Academy of Sciences. 2015; 112: 8199–8204. https://doi.org/10.1073/pnas.1423917112 PMID: 26056296

30. Martiny AC, Pham CTA, Primeau FW, Vrugt JA, Moore JK, Levin SA, et al. Strong latitudinal patterns in the elemental ratios of marine plankton and organic matter. Nature Geosci. 2013; 6: 279–283. https://doi.org/10.1038/ngeo1757

31. Bernardello R, Marinov I, Palter JB, Sarmiento JL, Galbraith ED, Slater RD. Response of the Ocean Natural Carbon Storage to Projected Twenty-First-Century Climate Change. Journal of Climate. 2014; 27: 2033–2053. https://doi.org/10.1175/JCLI-D-13-00343.1

32. Eggleston S, Galbraith ED. The devil's in the disequilibrium: multi-component analysis of dissolved carbon and oxygen changes under a broad range of forcings in a general circulation model. Biogeosciences. 2018; 15: 3761–3777. https://doi.org/10.5194/bg-15-3761-2018

33. Nowicki M, DeVries T, Siegel DA. The Influence of Air-Sea CO2 Disequilibrium on Carbon Sequestration by the Ocean's Biological Pump. Global Biogeochemical Cycles. 2024; 38: e2023GB007880. https://doi.org/10.1029/2023GB007880

34. Schmittner A, Bostock HC, Cartapanis O, Curry WB, Filipsson HL, Galbraith ED, et al. Calibration of the carbon isotope composition (δ13C) of benthic foraminifera. Paleoceanography. 2017; 32: 512–530. https://doi.org/10.1002/2016PA003072

35. Shackleton NJ. Carbon-13 in Uvigerina: Tropical rain forest history and the equatorial Pacific carbonate dissolution cycle. The fate of fossil fuel CO_2 in the oceans. 1977; 401–428.

36. Ciais P, Tagliabue A, Cuntz M, Bopp L, Scholze M, Hoffmann G, et al. Large inert carbon pool in the terrestrial biosphere during the Last Glacial Maximum. Nature Geosci. 2012; 5: 74–79. https://doi.org/10.1038/ngeo1324

37. Peterson CD, Lisiecki LE, Stern JV. Deglacial whole-ocean δ13C change estimated from 480 benthic foraminiferal records. Paleoceanography. 2014; 29: 549–563. https://doi.org/10.1002/2013PA002552

38. Brovkin V, Hofmann M, Bendtsen J, Ganopolski A. Ocean biology could control atmospheric δ13C during glacial-interglacial cycle. Geochemistry, Geophysics, Geosystems. 2002; 3: 1–15. https://doi.org/10.1029/2001GC000270

39. Mengis N, Keller DP, MacDougall AH, Eby M, Wright N, Meissner KJ, et al. Evaluation of the University of Victoria Earth System Climate Model version 2.10 (UVic ESCM 2.10). Geoscientific Model Development. 2020; 13: 4183–4204. https://doi.org/10.5194/gmd-13-4183-2020

40. Muglia J, Somes CJ, Nickelsen L, Schmittner A. Combined Effects of Atmospheric and Seafloor Iron Fluxes to the Glacial Ocean. Paleoceanography. 2017; 32: 1204–1218. https://doi.org/10.1002/2016PA003077

41. Muglia J, Skinner LC, Schmittner A. Weak overturning circulation and high Southern Ocean nutrient utilization maximized glacial ocean carbon. Earth and Planetary Science Letters. 2018; 496: 47–56. https://doi.org/10.1016/j.epsl.2018.05.038

42. Muglia J, Schmittner A. Glacial Atlantic overturning increased by wind stress in climate models. Geophysical Research Letters. 2015; 42: 9862–9868. https://doi.org/10.1002/2015GL064583

43. Muglia J, Schmittner A. Carbon isotope constraints on glacial Atlantic meridional overturning: Strength vs depth. Quaternary Science Reviews. 2021; 257: 106844. https://doi.org/10.1016/j.quascirev.2021.106844

44. Fillman N, Schmittner A, Kvale KF. Variable Stoichiometry Effects on Glacial/Interglacial Ocean Model Biogeochemical Cycles and Carbon Storage. Paleoceanography and Paleoclimatology. submitted manuscript.

45. Bauska TK, Baggenstos D, Brook EJ, Mix AC, Marcott SA, Petrenko VV, et al. Carbon isotopes characterize rapid changes in atmospheric carbon dioxide during the last deglaciation. Proceedings of the National Academy of Sciences. 2016; 113: 3465–3470. https://doi.org/10.1073/pnas.1513868113 PMID: 26976561

46. Bauska TK, Baggenstos D, Brook EJ, Mix AC, Marcott SA, Petrenko VV, et al. Carbon isotopes characterize rapid changes in atmospheric carbon dioxide during the last deglaciation. Proceedings of the National Academy of Sciences. 2016; 113: 3465–3470. https://doi.org/10.1073/pnas.1513868113 PMID: 26976561

47. Zeng N. Glacial-interglacial atmospheric CO2 change—The glacial burial hypothesis. Adv Atmos Sci. 2003; 20: 677–693. https://doi.org/10.1007/BF02915395

48. Bereiter B, Eggleston S, Schmitt J, Nehrbass-Ahles C, Stocker TF, Fischer H, et al. Revision of the EPICA Dome C CO2 record from 800 to 600 kyr before present. Geophysical Research Letters. 2015; 42: 542–549. https://doi.org/10.1002/2014GL061957

49. Annan JD, Hargreaves JC. A new global reconstruction of temperature changes at the Last Glacial Maximum. Climate of the Past. 2013; 9: 367–376. https://doi.org/10.5194/cp-9-367-2013

50. Bereiter B, Shackleton S, Baggenstos D, Kawamura K, Severinghaus J. Mean global ocean temperatures during the last glacial transition. Nature. 2018; 553: 39–44. https://doi.org/10.1038/nature25152 PMID: 29300008

51. Tierney JE, Zhu J, King J, Malevich SB, Hakim GJ, Poulsen CJ. Glacial cooling and climate sensitivity revisited. Nature. 2020; 584: 569–573. https://doi.org/10.1038/s41586-020-2617-x PMID: 32848226

52. Gebbie G, Peterson CD, Lisiecki LE, Spero HJ. Global-mean marine δ13C and its uncertainty in a glacial state estimate. Quaternary Science Reviews. 2015; 125: 144–159. https://doi.org/10.1016/j.quascirev.2015.08.010

53. Carter BR, Feely RA, Lauvset SK, Olsen A, DeVries T, Sonnerup R. Preformed Properties for Marine Organic Matter and Carbonate Mineral Cycling Quantification. Global Biogeochemical Cycles. 2021; 35: e2020GB006623. https://doi.org/10.1029/2020GB006623

54. Kwon EY, Timmermann A, Tipple BJ, Schmittner A. Projected reversal of oceanic stable carbon isotope ratio depth gradient with continued anthropogenic carbon emissions. Commun Earth Environ. 2022; 3: 1–12. https://doi.org/10.1038/s43247-022-00388-8

55. Lauvset SK, Key RM, Olsen A, van Heuven S, Velo A, Lin X, et al. A new global interior ocean mapped climatology: the 1˚ × 1˚ GLODAP version 2. Earth System Science Data. 2016; 8: 325–340. https://doi.org/10.5194/essd-8-325-2016

56. Olsen A, Key RM, van Heuven S, Lauvset SK, Velo A, Lin X, et al. The Global Ocean Data Analysis Project version 2 (GLODAPv2)–an internally consistent data product for the world ocean. Earth System Science Data. 2016; 8: 297–323. https://doi.org/10.5194/essd-8-297-2016

57. Curry WB, Oppo DW. Glacial water mass geometry and the distribution of δ13C of ΣCO2 in the western Atlantic Ocean. Paleoceanography. 2005; 20. https://doi.org/10.1029/2004PA001021

58. Duplessy JC, Shackleton NJ, Fairbanks RG, Labeyrie L, Oppo D, Kallel N. Deepwater source variations during the last climatic cycle and their impact on the global deepwater circulation. Paleoceanography. 1988; 3: 343–360. https://doi.org/10.1029/PA003i003p00343

59. Eide M, Olsen A, Ninnemann US, Johannessen T. A global ocean climatology of preindustrial and modern ocean δ13C. Global Biogeochemical Cycles. 2017; 31: 515–534. https://doi.org/10.1002/2016GB005473

60. Boyle EA. Vertical oceanic nutrient fractionation and glacial/interglacial CO2 cycles. Nature. 1988; 331: 55–56. https://doi.org/10.1038/331055a0

61. Brovkin V, Ganopolski A, Archer D, Rahmstorf S. Lowering of glacial atmospheric CO2 in response to changes in oceanic circulation and marine biogeochemistry. Paleoceanography. 2007;22. https://doi.org/10.1029/2006PA001380

62. Cartapanis O, Bianchi D, Jaccard SL, Galbraith ED. Global pulses of organic carbon burial in deep-sea sediments during glacial maxima. Nat Commun. 2016; 7: 10796. https://doi.org/10.1038/ncomms10796 PMID: 26923945

63. Key RM, Kozyr A, Sabine CL, Lee K, Wanninkhof R, Bullister JL, et al. A global ocean carbon climatology: Results from Global Data Analysis Project (GLODAP). Global Biogeochemical Cycles. 2004; 18. https://doi.org/10.1029/2004GB002247

64. Garcia HE, Locarnini RA, Boyer TP, Antonov JI, Baranova OK, Zweng MM, et al. World Ocean Atlas 2013. Volume 4, Dissolved inorganic nutrients (phosphate, nitrate, silicate). 2013 [cited 12 Feb 2024]. https://doi.org/10.7289/V5J67DWD